Artificial Organs
27(12):1102–1109, Blackwell Publishing, Inc.

Diaphragm Motion Affects Flow Patterns in an Artificial Heart

*Pramote Hochareon, *Keefe B. Manning, †Arnold A. Fontaine, †Steven Deutsch, and *John M. Tarbell

**Department of Bioengineering and †Applied Research Laboratory, Artificial Heart Laboratory, The Pennsylvania State University, University Park, PA, U.S.A.*

Abstract: In the sac-driven artificial heart, the flow characteristics are coupled to the dynamics of the sac motion. The opening dynamics of the sac wall can, for example, strongly affect the chamber flow characteristics during diastole by directing or impeding the inflow. Poor sac motion can reduce the volume output of the pump and may increase the potential for thrombus formation within the ventricular chamber. It is particularly important for laboratory studies of the flow fields in artificial hearts that the diaphragm motion properly simulates the sac motion observed in vivo. In the present study, flow visualization was performed to investigate the relationship between the chamber flow characteristics of a Penn State artificial heart and the motion of the diaphragm during the filling phase during in vitro experimentation. The chamber flow pattern and diaphragm motion were recorded as a function of time, using high-speed videography. Experiments were conducted to determine the influence of diaphragm motion on the flow characteristics by altering the filling pressure, diaphragm thickness, and fluid density. Diaphragm motion was quantified by tracking the position of three surface points over the cardiac cycle. The alignment of these three surface trajectories can be used to quantify the uniformity of diaphragm motion. As a result, diaphragm motion was determined to be nonuniform under most operating conditions with the diaphragm opening in a wave-like pattern starting at the bottom of the chamber and propagating toward the inflow/outflow ports. This opening pattern simulates the opening pattern observed in an in vitro study of the clinical blood sac used in the Lionheart LVAD. **Key Words: ••**

1

The dynamics of blood flow in an artificial heart are potentially responsible for complications after implantation. An understanding of the inflow dynamics coupled with the characteristics of sac motion is needed to design a sac geometry and housing that will ensure favorable operating conditions over long duration. Because of the complexity of sac-type artificial heart geometries, turbulence flow fields, and fluid–solid interactions, computational fluid dynamics, in its current state of development, is of limited use in studying the coupled problem. There has been, however, a good deal of experimental work on the flow field characteristics of piston-driven artificial hearts. Jarvis et al. (1) and Baldwin et al. (2–4) have studied the in vitro fluid dynamics of the Penn State artificial heart. In their studies, a transparent plastic test model, with an identical inner geometry to the implanted artificial heart, was fabricated in order to allow optical access. Most of their measurements focused on fluid dynamic phenomena and disregarded the behavior of the diaphragm during a cycle. Other computational and experimental fluid dynamic studies of sac-type artificial hearts (5–10) have not established the relationship between the pump flow field and diaphragm motion either. In all of the previous studies, the sac motion was assumed to play a passive role during filling with little impact on the chamber flow characteristics. The objective of this study was to investigate the relationship between the diaphragm motion and the flow. Because most of the undesired mechanically induced biochemical processes, such as protein deposition, platelet activa-

Received October 2002; revised February 2003.
Address correspondence and reprint requests to Dr. Steven Deutsch, Artificial Heart Laboratory, The Pennsylvania State University, 205 Hallowell Building, University Park, PA 16802, U.S.A. E-mail: SD1@wt.arl.psu.edu

tion and deposition, and clot formation, are probably activated during the diastolic phase, our study concentrates on the filling phase. With this in mind, we use the term "diaphragm opening" interchangeably with "diaphragm motion."

MATERIALS AND METHODS

The 70-cc Penn State artificial heart test chamber was made of transparent Plexiglas and was machined to be identical to the geometry of the front half of the implantable 70-cc artificial heart blood sac. Unlike the fully flexible blood sac of the implanted artificial heart, the in vitro test model had only half of a sac on the pusher plate side of the chamber. However, the front half, opposite to the pusher plate, of the clinical whole sac does not move very much during a beat cycle. Therefore, our semiflexible model simulates the fluid dynamics and the sac motion within the sac. We will refer to the half blood sac in the in vitro test model as a diaphragm. Figure 1 shows the configuration of the in vitro model. A polyurethane diaphragm covered the open half of the Plexiglas model. Bjork-Shiley (Shiley Inc., Irvine, CA, U.S.A.) monostrut valves with pyrolytic carbon discs were used at the mitral (#29) and aortic (#27) ports to achieve unidirectional flow. The pusher plate, which compressed the blood sac, was driven by a piston pump (Harvard Apparatus Co., Inc., Millis, MA, U.S.A.). The flow loop, which has been described previously, contained inlet and outlet piston-type compliance chambers (11), which simulated the atrial and aortic compliance. A parallel plate resistor downstream of the aortic compliance simulated the systemic resistance. A reservoir between the systemic resistance and the atrial compliance controlled preload to the chamber. Pressure waveforms at the inlet and outlet compliance chambers

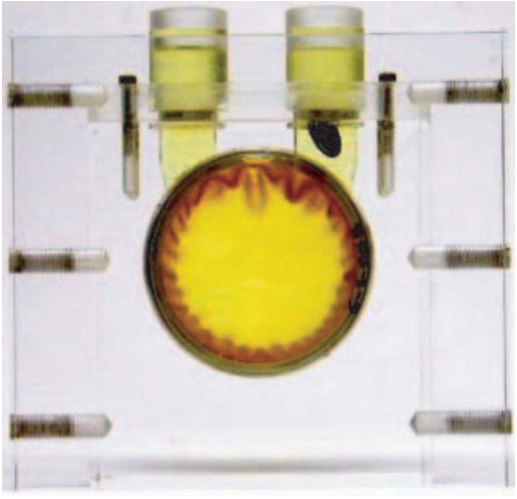

a)

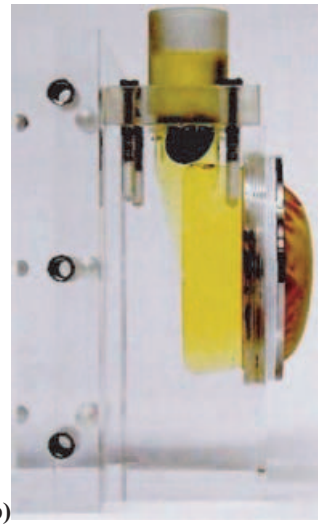

b)

c)

FIG. 1. The configuration of the *in vitro* model: (a) front view, (b) side view (frontal edge of the chamber is on the left), and (c) back view. (The yellow solution indicates where the chamber is within the model.)

were monitored by pressure transducers (Maxxim Medical Inc., Athens, TX, U.S.A.). Two ultrasonic flow meters (model T110R, Transonic System Inc., Ithaca, NY, U.S.A.) were used to record flow waveforms at the inlet and outlet ports. The test fluid was composed of 79% saturated aqueous NaI solution, 20% glycerin, and 1% water, by volume. The fluid had a kinematic viscosity of 3.77 centistokes, a density of 1.74 g/cc, and a refractive index of 1.49 (nearly matching the refractive index of the Plexiglas). The flow was seeded with stainless steel-coated hollow glass beads (3M, Minneapolis, MN, U.S.A.), with a diameter of 50 μm and specific gravity of 0.86. The particle size was sufficiently small to minimize the relative velocity between the particle and the fluid (12,13), while still reflecting sufficient light for flow visualization. A continuous 5-W argon-ion laser (Spectra Physics, Mountain View, CA, U.S.A.) and appropriate cylindrical lens were used to form a 1.5-mm-thick light sheet as shown in Fig. 2. The particle motion was captured by a Kodak high-speed video camera (Kodak Motion Corder Analyzer, San Diego, CA, U.S.A.), operating at 250 frames per second.

Nine different experimental conditions were investigated to determine the relationship between flow patterns and diaphragm opening motion during diastole. The experiments and their associated parameters, which are given in Table 1, considered the influence of a diaphragm attached to the pusher plate vs. a free (unattached) diaphragm, and, for a free diaphragm, investigated the influence of inlet pressure, diaphragm thickness, initial diaphragm stress (prestressing) and fluid density. Fluid density is of interest because of its influence on fluid inertia during pump filling.

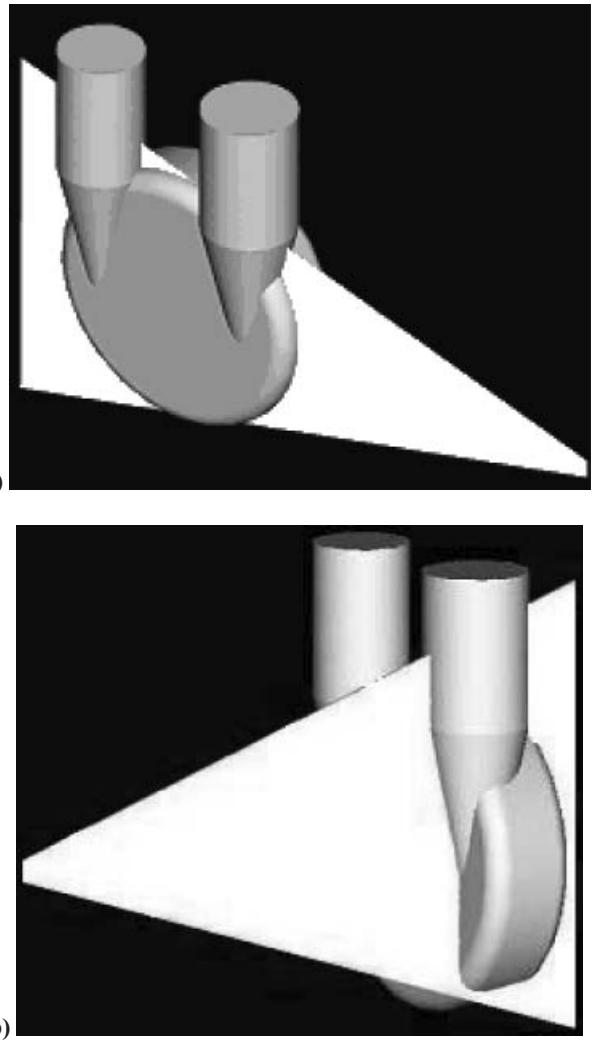

FIG. 2. Light sheet orientation: (a) middle and (b) sagittal plane.

RESULTS AND DISCUSSION

To study the relationship between diaphragm motion and flow, we set up a controlled experiment to create a uniform diaphragm opening pattern, by gluing the diaphragm to the surface of the pusher plate. In Fig. 3a, we show the inlet and outlet flow waveforms; in Fig. 3b, photographs of the diaphragm

TABLE 1. *Case descriptions and operating conditions*

Case number: case description	Outlet pressure (mm Hg)	Inlet pressure (mm Hg)	Peak outflow (L/min)	Peak inflow (L/min)	Mean flow rate (L/min)	Beat rate/min	Stroke volume (mL)
1: 70-cc chamber with glued diaphragm	130/75	25/9	20.5	22	4.6	75	61.27
2: 70-cc chamber with thick unglued diaphragm	130/75	26/12	20	12.2	4.8	76	63.83
3: case 2 with 20 mm Hg peak inlet pressure	130/75	17/07	18	12	3.89	67	58.4
4: case 2 with 30 mm Hg peak inlet pressure	130/80	32/22	18.5	12.5	4.15	67	61.74
5: case 2 with 40 mm Hg peak inlet pressure	130/80	40/20	19	20	4.3	67	64.16
6: case 2 with 55 mm Hg peak inlet pressure	130/75	55/25	19.5	22	4.64	68	67.76
7: 70-cc chamber with thin unglued diaphragm	125/75	25/10	20	13	4.92	75	65.29
8: case 7 but using 40% glycerin in water for the test fluid	120/70	25/8	21	12	3.94	73	53.63
9: 70-cc chamber with 50-cc diaphragm	125/75	25/8	20	15	4.99	75	66.71

All cases used the 70-cc-size diaphragm, unless specified. NaI was used as the test fluid in all cases unless specified.

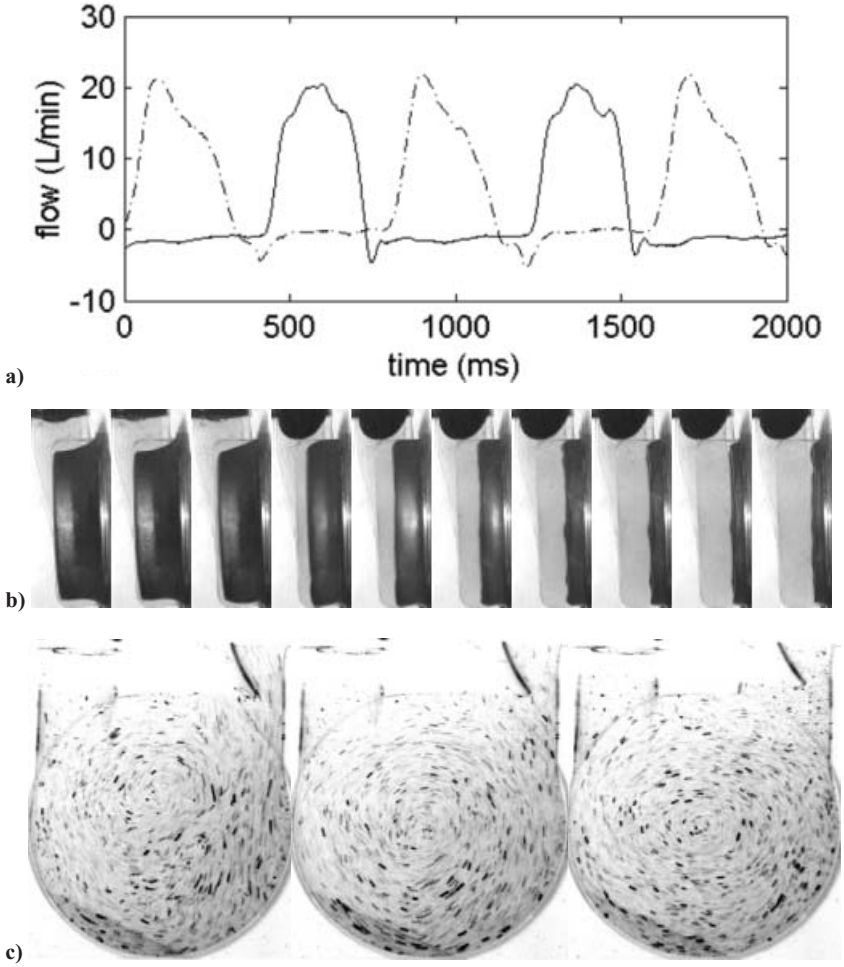

FIG. 3. Case 1, 70-cc chamber with glued diaphragm. (a) Dashed line = outflow waveform; solid line = inflow waveform. (Time 0 is the beginning of systole.) (b) Sequence of diaphragm motion from 370 to 710 ms (40 ms increment), left to right, respectively. (The left side of each photograph is the front edge and the right side is where the pusher plate is located.) (c) Snap shots of the main vortex from flow visualization of case 1, at 500, 600, and 700 ms, corresponding to the fifth, seventh, and last snap shots from (b).

motion are displayed; and in Fig. 3c, particle streakline images of the flow field at several instants of time during diastole are displayed. Figure 3b shows that we have achieved uniform diaphragm motion during the filling phase. Figure 3c shows that the uniform diaphragm motion induces a single vortex motion throughout diastole. Baldwin et al. (2,4) showed a similar vortex pattern, using extensive Laser Doppler velocimetry measurements, in a comparable artificial heart design. Baldwin et al. (4) indicated that this single vortex flow pattern provides good wall washing, which may help to minimize clot formation.

We note that the inflow waveform in Fig. 3a does not show a plateau phase—that is, a period of sustained, nearly constant, flow to the heart that is typically observed in animal experiments (14). In addition, for this glued diaphragm case, the inflow peak is comparable to the outflow peak. The inflow waveform in Fig. 3a is not, however, characteristic of the "free diaphragm" artificial heart waveforms. The atypical high inflow peak is probably a result of the negative pressure gradient created by the pusher plate pulling the diaphragm. The primary goal of the glued sac experiment was to investigate the induced flow pattern generated by a sac that was constrained to move with the piston. The changes in the inflow patterns that were observed are most likely due to the reduced sac obstruction even though the inflow waveforms were different. The inflow waveforms can be controlled if the piston is controlled to move in a certain pattern. We may then be able to obtain the physiologic waveform while maintaining control of sac motion and inflow patterns within the chamber. Nevertheless, the feasibility of maintaining the integrity of an attached clinical sac may have to be investigated from a fatigue standpoint.

The second condition with a free diaphragm yielded an inflow waveform with the anticipated plateau phase, as shown in Fig. 4a. The diaphragm opening for this case was nonuniform, as detailed in Fig. 4b, with the diaphragm opening at the bottom of the chamber (location away from the valves) first

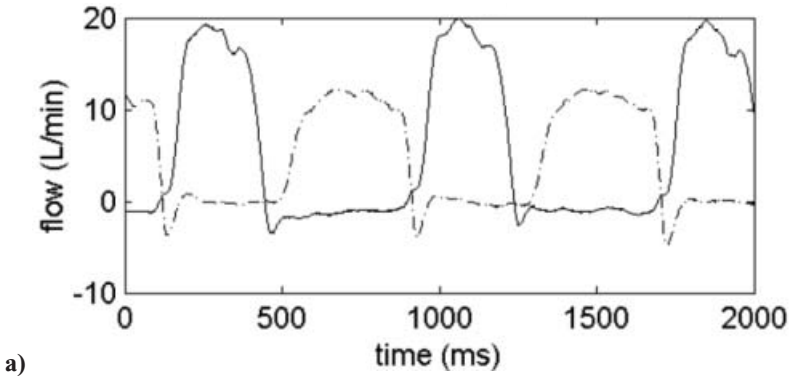

a)

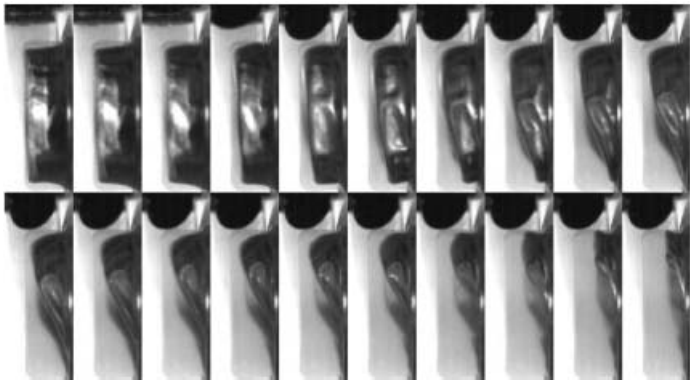

b)

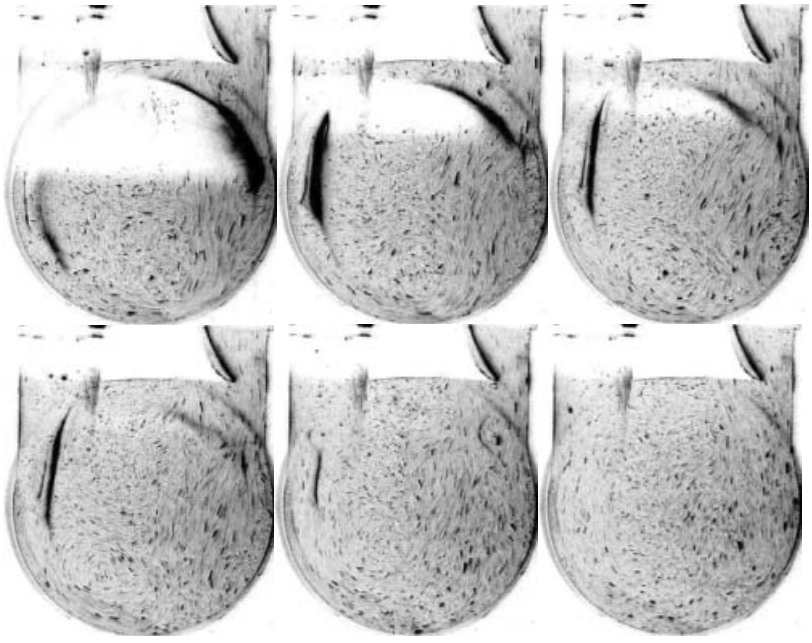

c)

FIG. 4. Case 2, 70-cc chamber with thick unglued diaphragm. (a) Dashed line = outflow waveform; solid line = inflow waveform. (Time 0 is the beginning of systole.) (b) Sequence of diaphragm motion from 350 to 730 ms (20 ms increment), left to right, respectively. (The left side of each photograph is the front edge and the right side is where the pusher plate is located.) (c) Snap shots of the main vortex from flow visualization of case 2, at 500 (second snap shot from the right in the first row of (b)), 550, 600 (third snap shot from the left in the second row of [b]), 650, 700 (third snap shot from the right on the second row of (b)) and 800 ms (right before the ejection).

while the top part of the diaphragm did not open until late diastole. This opening pattern correlated well with the pattern observed with the clinical blood sac of a Lionheart LVAD recorded at Arrow Inc. (unpublished flow visualization recording; Reading, PA, U.S.A.). Flow visualization shows a vortex that grows with the open volume of the diaphragm (Fig. 4c). That is, a smaller vortex is initially formed in the open area at the bottom of the sac, and the center of this vortex moves up and becomes larger as the open volume increases. At the end of diastole, the vortex occupies almost the entire chamber. Because

the pattern has been observed within the Lionheart, this suggests that the vortex flow pattern that grows during diastole provides a quasistable flow field that may be nontraumatic to blood elements. However, we were not able to determine the critical factors that dictate the diaphragm motion pattern, which would help us to understand the mechanism of wall–fluid coupling better. Because this was a preliminary study of the wall–fluid coupling problem of sac-type artificial hearts, we have not ruled out the material properties of the sac or the nature of pressure driving flow as contributing factors to the sac opening dynamics. Nonlinear sac mechanics, such as buckling of the edge of the diaphragm, may affect diaphragm opening in subtle ways. Atrial compliance, which modulates driving pressure to the chamber, may also impact the coupling phenomena. Another influential factor may be the geometry of the inlet port and mitral valve, which alter the flow characteristics entering the main chamber. There is, however, a significant amount of small-scale motion, not found in either experiment 1 (Fig. 3c) or the results of Baldwin et al. (2,4). Intuitively, we associate such small-scale motion with increased dissipation and thereby, a less efficient filling.

To help quantify the correlation between flow patterns and diaphragm motion, we use the photographic history (e.g., Figs. 3b and 4b) to measure the distance from the frontal edge of the chamber to the instantaneous diaphragm position as a function of time at three locations: 2 cm from the top, the center, and 2 cm from the bottom of the chamber. Those data are presented in normalized form (% opening, with respect to the full open position) against cycle time (Fig. 5). Figure 5a shows the opening pattern of the glued diaphragm. The diaphragm trajectories at the three locations of the diaphragm overlie each other, indicating a uniform opening pattern. Figure 5b illustrates the nonuniform opening pattern of the free diaphragm. It quantitatively shows that the bottom part of the diaphragm opened earlier, and that there is a significant difference in the open volume between the top and the bottom section during the first half of diastole. The top part fully opens for only the last 20% of diastole. The positive slope of each curve also implies the relative opening speed for each part of the diaphragm. It is clear that the bottom part opens much faster than the top part.

Next, we varied the maximum inlet pressure from 20 to 55 mm Hg to study its effect on the diaphragm opening pattern and the associated fluid mechanics. Figure 6a,b presents the comparison of inflow waveforms and diaphragm trajectories for four cases. Surprisingly, the inflow waveforms are similar for the 20

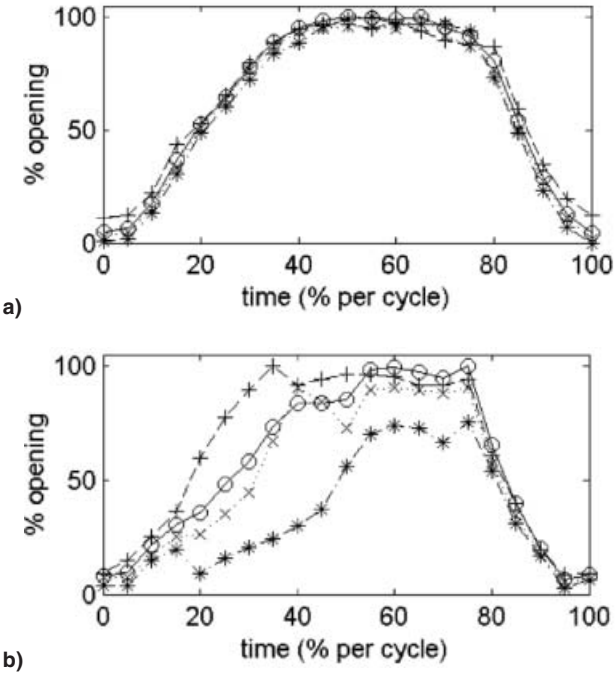

FIG. 5. Diaphragm motion plots, the trajectories of the three locations of the diaphragm: (a) case 1, (b) case 2. (–∗–) is the bottom part trajectory, (–×–) is the center part trajectory, (–+–) is the top part trajectory, and (–○–) is the calculated % open volume. (Time 0% is the beginning of diastole.)

and 30 mm Hg cases and for the 40 and 55 mm Hg cases, but the two groups are quite different in flow characteristics. Based upon the inflow pattern, one might have expected the diaphragm trajectory patterns within each group (20/30 and 40/55 mm Hg) to be similar but different between groups. However, the diaphragm opening data of Fig. 6b show that the 40 mm Hg case is similar to the 20 and 30 mm Hg cases rather than to the 55 mm Hg case, which is much more uniform. Interestingly, the visualized fluid motion of the first three cases (20, 30, and 40 mm Hg) are indistinguishable from each other (also from the results of experiment 2, Fig. 4c). Flow visualization for the 55 mm Hg case, however, shows an early single vortex, which is similar to that of the fixed diaphragm case (compare Fig. 6c and Fig. 3c). This observation suggests the diaphragm opening patterns are correlated more to the flow patterns than the inflow waveforms, and, most importantly, indicates that inflow waveform alone is not adequate to anticipate the flow characteristics.

The effect of the diaphragm thickness on the diaphragm motion was also studied by manufacturing and testing a much thinner diaphragm. The thicknesses for the thick diaphragm were 0.4318, 0.254, and 0.3048 mm for the flat center, circumferential

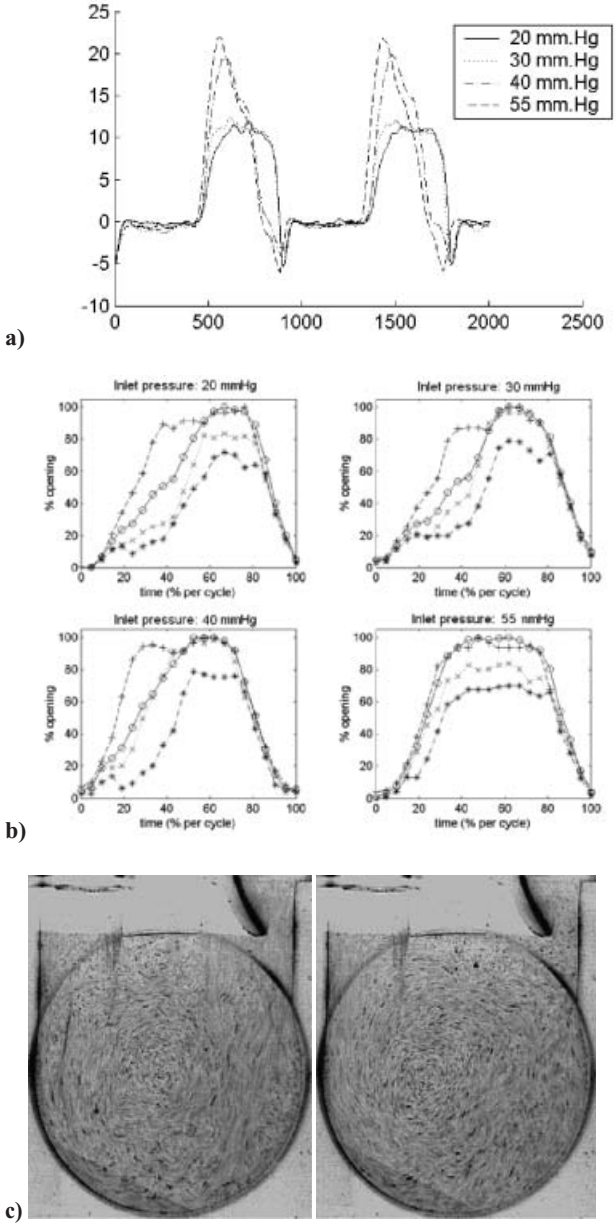

FIG. 6. Effect of filling pressure (cases 3–6). (a) Inflow waveform. (b) Diaphragm motion trajectories. (c) Snap shots from flow visualization of case 6 at 550 and 700 ms corresponding to the beginning through the end of diastole. (Time 0 ms in (a) is the beginning of systole; time 0% in (b) is the beginning of diastole.)

hinge, and circumferential edge of the diaphragm, respectively; and for the thin diaphragm, thicknesses were 0.3683, 0.2032, and 0.254 mm, respectively. Figure 7 shows the opening pattern for the thin diaphragm case. It is much like the pattern of case 2 (Fig. 5b), and we may therefore conclude that, within limits, the thickness of the diaphragm is not critical in determining the sac opening characteristics. A similar outcome was obtained for a case in which an

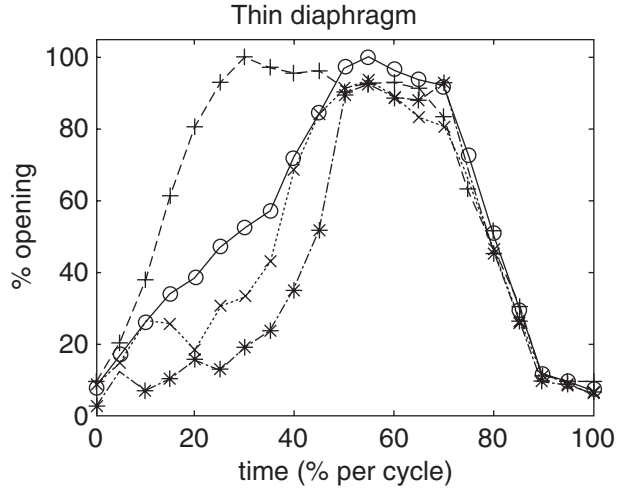

FIG. 7. Effect of diaphragm thickness (case 7, thin 70-cc diaphragm). (Time 0% is the beginning of diastole.)

undersized diaphragm was prestressed by stretching it to fit within the heart pump. The results are shown in Fig. 8, which again are much like those in case 2.

The density of the test fluid was another parameter of interest. We routinely use the higher density (1.74 kg/m^3) NaI solution to match the refractive index between the fluid and the heart model. Figure 9 shows the opening pattern from the experiment using 40% glycerin in water (1 kg/m^3 density) as a test fluid. The opening trajectories for different density fluids were similar (compare Fig. 7 and Fig. 9).

Changes in prestretch, diaphragm thickness, and fluid density minimally affect the diaphragm motion and thus the vortex pattern developing during diastole. Only a high maximum inlet pressure of 55 mm Hg altered the diaphragm motion by creating

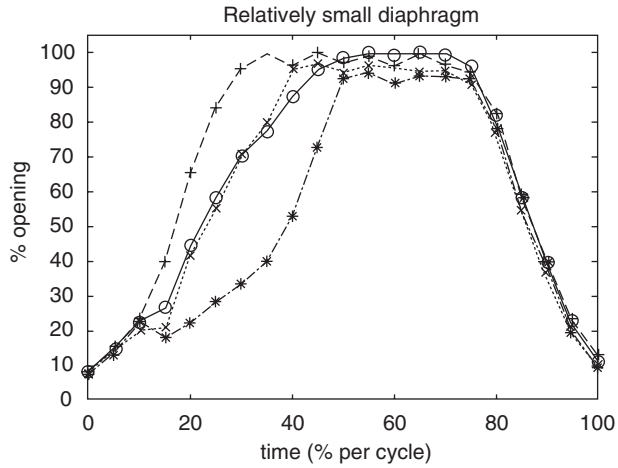

FIG. 8. Effect of diaphragm resting stress (case 8). (Time 0% is the beginning of diastole.)

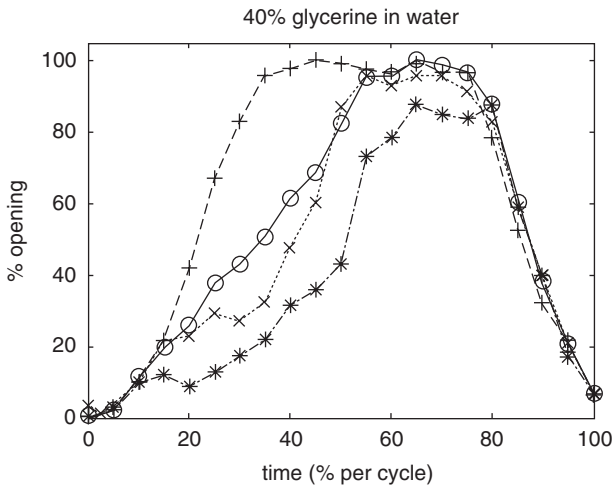

FIG. 9. Effect of fluid density (case 9). (Time 0% is the beginning of diastole.)

a more uniform motion similar to the glued sac experiment. Perhaps the cause of the nonuniform diaphragm motion may be related to the chamber orientation whereby fluid enters the chamber at the top and immediately settles at the bottom of the chamber and moves in an increasing vortex pattern as more fluid enters the chamber. Evaluating the chamber in a plane parallel to the gravitational field might elucidate further explanations to the diaphragm motion affecting fluid dynamics. Furthermore, the flow within the chamber may be influenced by the geometry of the inflow port.

CONCLUSIONS

We have found that the diaphragm motion patterns more accurately reflect the fluid dynamics within the artificial heart chamber than do other flow properties, such as inlet pressure or inflow waveform. The nonuniform diaphragm opening pattern controls the vortex flow pattern within the pumping chamber, which may affect the hematological performance of the pump. More importantly, we can use the diaphragm motion, which is obtainable from animal experiments, as another parameter to ensure the matching of conditions between in vitro fluid mechanical and in vivo biological experiments, where direct and accurate qualitative flow visualization is not achievable. The quantification of the diaphragm trajectory patterns has been introduced as a new method to describe pump filling, which is indicative of pump flow patterns that may influence blood interactions. The delay and speed of the opening of the top part of the diaphragm relative to the bottom part seems to be one of the critical features that correlate with the flow pattern. Whether or not improved diaphragm opening dynamics can lead to improved flow patterns within the pumping chamber and better hematological performance will be determined in future studies.

Acknowledgment: This project is funded by the NIH NHLBI grant HL 60276.

REFERENCES

1. Jarvis P, Tarbell JM, Frangos JA. An in vitro evaluation of an artificial heart. *ASAIO Trans* 1991;37:27–32.
2. Baldwin JT, Deutsch S, Geselowitz DB, Tarbell JM. Mean flow velocity patterns within a ventricular assist device. *ASAIO Trans* 1988;35:429–33.
3. Baldwin JT, Deutsch S, Geselowitz DB, Tarbell JM. Estimation of Reynolds stresses within the Penn State left ventricular assist device. *ASAIO Trans* 1990;36:M274–8.
4. Baldwin JT, Deutsch S, Geselowitz DB, Tarbell JM. LDA measurements of mean velocity and Reynolds stress fields within an artificial heart ventricle. *J Biomech Eng* 1994;116:190–9.
5. Rogers SE, Kutler P, Kwak D, Kiris C. *Numerical Simulation of Flow Through an Artificial Heart.* NASA Technical Memorandum 102183, April 1989.
6. Kiris C, Rogers SE, Kwak D, Chang ID. Computation of compressible viscous flows through artificial heart devices with moving boundaries. *Contem Math* 1991.
7. Clark C, Jin W, Glaser A. The fluid mechanics of a sac-type ventricular assist device. *Int J Artif Organs* 1990;13:814–22.
8. Jin W, Clark C. Experimental investigation of unsteady flow behavior within a sac-type ventricular assist device (VAD). *J Biomech* 1993;26:697–707.
9. Jin W, Clark C. Pressure development within a sac-type pneumatically driven ventricular assist device. *J Biomech* 1994;27:1319–29.
10. Jin W, Clark C. Experimental investigation of the pumping diaphragm within a sac-type pneumatically driven ventricular assist device. *J Biomech* 1994;27:43–55.
11. Rosenberg G, Phillips WM, Landis DL, Pierce WS. Design and evaluation of the Pennsylvania State University Mock Circulatory System. *ASAIO Trans* 1981;4:41–9.
12. Merzkirch W. *Flow Visualization*. New York: Academic Press, 1974.
13. Raffel M, Willert C, Kompenhans J. *Particle Imaging Velocimetry: A Practical Guide*. New York: Springer, 1998.
14. Guyton AC, Hall JE. *Textbook of Medical Physiology*. Philadelphia, PA: W.B. Saunders, 2000.